Electrochimica Acta 488 (2024) 144190

Contents lists available at ScienceDirect

Electrochimica Acta

journal homepage: www.journals.elsevier.com/electrochimica-acta

Improved plating/stripping in anode-free lithium metal batteries through electrodeposition of lithiophilic zinc thin films

Pooria Afzali, Eugenio Gibertini, Luca Magagnin *

Dipartimento di Chimica, Materiali e Ingegneria Chimica "Giulio Natta", Politecnico di Milano, Via Luigi Mancinelli 7, Milan 20131, Italy

ARTICLE INFO

Keywords:
AFLB
Lithiophilicity
Electrochemical deposition
Dendrites
GITT

ABSTRACT

The new concept of anode-free Li batteries (AFLBs) with no excess lithium, while retaining numerous strengths, does come with certain challenges, such as high capacity loss and low coulombic efficiency. These challenges can be addressed through the utilization of modified lithiophilic current collectors to enhance the electrochemical performances. Herein, we investigated the surface modification of the Cu current collector by zinc electrodeposition to provide a lithiophilic thin layer. This process aims to facilitate a smoother plating/stripping process, leading to a uniform and dendrite-free lithium deposition on the Li_xZn_y phase formed at the first stages of plating. The zinc-modified current collectors improved cell's performances, including smooth and dense lithium deposition, reduced overpotential at various applied current densities (44.5 mV to 16.8 mV @0.25 mA cm^{-2}), prolonged cycling stability for about 300 cycles and provided high coulombic efficiency of 95 % when compared to bare Cu electrodes. These improvements are attributed to a favorable lithium alloying reaction on the Zn-coated surface. Galvanostatic Intermittent Titration Technique (GITT) and Electrochemical Impedance Spectroscopy (EIS) revealed high diffusion coefficients for lithium (ranging from 10^{-9} to 10^{-6} cm^2 s^{-1}), despite of the solid-state Li diffusion in the Zn film coating. We anticipate that implementing this modified current collector in a half-cell configuration could lead to the realization of a high-performance, anode-free lithium battery. This holistic approach proposes a scalable and cost-effective technique for boosting the performance of AFLBs.

1. Introduction

To develop advanced portable electrical devices and hybrid electric vehicles (HEVs), more efficient energy storages and battery systems with higher energy density at reduced cost, are required [1–3]. Unluckily, conventional Li-ion batteries (LIBs), possessing an energy density of 250–300 Wh kg^{-1}, are quickly approaching their capacity limit and will hardly meet the tremendous demand of newcoming energy storage applications [4,5]. Li-metal is known as a high energy density material with ideal theoretical capacity (3860 mAh g^{-1}) and low redox potential (−3.04 V vs SHE) [6]. Hence, such properties made lithium metal a promising anode material to be used instead of graphite. Nonetheless, such a high amount of excess lithium as anode active material can react with the electrolyte and can lead to rapid consumption of electrolyte and growth of Li nucleation sites which results in the dendritic growth of lithium. During further Li plating-stripping, dendrites may cause short circuits and intensify the accumulation of dead Li in the solid electrolyte interphase (SEI). Hence, a high rate of capacity loss, lower coulombic efficiency and hazardous safety issues can occur [6–10]. Due to the aforementioned challenges, the new concept of anode-free lithium battery (AFLB) has emerged. In this regard, an anode-free battery includes zero excess lithium on the anode and the copper current collector is directly in contact with the membrane (separator) in the absence of lithium foil. The elimination of lithium foil can provide high gravimetric and volumetric energy densities and reduced costs. Moreover, successive side reactions and thermal runaway are reduced and a safer battery cell can be achieved [11–13]. However, low coulombic efficiency and typical cyclability of around 40–50 cycles due to the zero excess lithium prevents the AFLBs to be functional [14–16]. In this regard, some strategies were found to be efficient in order to provide stable cycling behavior of AFLBs [17,18]. Columbic efficiency, reversibility of plated Li metal and long cyclability of AFLBs are highly affected by the electrolyte composition and unfavorable side reactions. Hence, electrolyte engineering is of great significance, especially for anode-free cells which has no excess source of lithium [19–21]. In this regard, many researchers have been working on different electrolyte compositions in order to regulate the SEI layer formed on the anode surface by manipulating the solvent, additives and lithium salt selection [22,23]. According to

* Corresponding author.
E-mail address: luca.magagnin@polimi.it (L. Magagnin).

https://doi.org/10.1016/j.electacta.2024.144190
Received 8 February 2024; Received in revised form 27 March 2024; Accepted 28 March 2024
Available online 29 March 2024

reports, a durable quasi-solid electrolyte (QSE) made from thermoplastic polyurethane and nano-fumed silica aerogels offers mechanical strength, hydrophobicity, and thermal stability [24].Also, a recent work attributed uniform, dendrite-free Li deposition at the SEI/Li interface to the development of an artificial hybrid LiF/Li_3Sb SEI layer, enhancing Li diffusion [25]. Surface modification of the copper foil current collector is a further highly effective approach to enhance the poor and inhomogeneous lithium deposition on the copper sheet during plating [26]. For instance, it was found that an Au/rGO composite film facilitates an even distribution of the electric field across the anode surface, leading to smoother lithium plating [27] or porous substrate or a coated 3D layer on the current collector can embed higher lithium in the host matrix resulting in high active surface and longer life cycles [28–31]. Recently, three-dimensional SnO_2 film was coated on the copper current collector of LIBs to improve the electrochemical performance of the cell [32]. The other approach was to apply gallium-based liquid metal (LM) layer on the copper foil resulting in uniform lithium deposition and less dendrite formation [33]. However, the complex fabrication process of 3D current collectors and porous hosts requires a prolonged manufacturing period, making it not cost-effective for mass production [34]. In preference, inorganic coatings on the current collector by lithiophilic metals such as Zn, Mg, Ag, Sn, Au, Pt and etc., can significantly decrease the nucleation overpotential due to the higher lithium solubility in these metals [35–37]. Such findings proved that substrate materials and coatings applied (like Sn, Zn, Al, Pt, and Au) on the current collector can highly affect the nucleation overpotential and, as consequence, lithium plating/stripping behavior [38–41]. Developing an appropriate lithiophilic material through a cost-effective process for mass production of AFLBs would be essential [42,43]. Zinc seems to be a desirable choice based on its abundance and competitive price in comparison to other lithophilic metals. Zinc alloying with lithium forms different intermetallic phases, so that Li_xZn_y can provide high volumetric capacity and promising chemical diffusion [42,44]. Moreover, Zn can be alloyed with Cu current collector in different atomic ratios due to the relatively same atomic radius to copper. In spite of all aforementioned merits of Zn, only a few papers have been published on its application in lithium metal batteries and almost none on the AFLBs [44–47]. For instance, using in situ deposition of a zinc interlayer from a PEO-based SPE to modify the Cu current collector improved li plating/stripping [48].

Desiring to reduce nucleation overpotential and improve the cyclability and Li plating/stripping behavior on the Cu substrate for AFLBs, in this work we modified the Cu current collector with a thin Zn layer by a simple electroplating route. In fact, nevertheless Zn electroplating is a widely used industrial process, it was rarely employed for providing engineered current collector for AFLBs. The metallic Li can form a Li_xZn_y alloy in the initial cycles and in the further plating/stripping cycles, the Li can deposit smoothly on the pre-formed Zn-Li alloy surface. Such lithiophilic Zn layer effectively reduced the nucleation overpotential from 44.5 mV to 16.8 mV @0.25 mA cm^{-2} with a stable coulombic efficiency of 95 %. Electrochemical measurements showed that the increase of the Zn layer thickness (Zn loading) improved the cycling behavior of about 300 cycles.

2. Experimental

2.1. Preparation of Zn@Cu electrode

The copper foil (10 μm thick) before being coated was soaked in 0.06 M HNO_3 for 5 min then rinsed with deionized water to remove the native oxide layer. Zn electrodeposition bath consisted in 2.43 M of H_3NSO_3 and 0.2 M of $(ZnCo_3)_2(Zn(OH)_2)_3$. Solution pH was adjusted at 3.3 by adding NaOH. Electrodeposition was performed in galvanostatic mode at a current density of 45 mA cm^{-2} without stirring, using a custom-built frame to fix the thin Cu foil and a pure Zn strip as counter electrode. The Zn layer thickness electroplated was controlled by the deposition time to obtain different thicknesses of 300 nm (0.3Zn@Cu), 600 nm (0.6Zn@Cu) and 1 μm (1Zn@Cu). The Zn coated samples were finally rinsed with deionized water and further dried under nitrogen gas stream.

2.2. Electrochemical measurements

Cyclic voltammetry (CV), galvanostatic plating/stripping tests and electrochemical impedance spectroscopy (EIS) technique were used to understand the electrochemical behavior. Electrochemical analyses were performed assembling CR2032 coin cell batteries in an Ar-filled glove box with Celgard 2025 separator, Li foil as counter/reference electrode and Zn@Cu as the working electrode. Lithium bis(trifluoromethanesulfonyl)imide (LiTFSI) 1,3-dioxolane (DOL) and 1,2-dimethoxyethane (DME) (1:1 by volume) with 3 wt% $LiNO_3$ was used as the electrolyte (25 μl per cell). A graphical representation of the cell setup is depicted in Fig. S1. All the assembled cells before any electrochemical measurements were kept at open circuit condition for 3 h. Plating/stripping and columbic efficiency (CE) measurements were performed by cycling the cells for 5 cycles at 0.25 mA cm^{-2} for stabilizing the SEI film and then cycling the cells at different current densities fixing the capacity to 1 mAh cm^{-2}. Cyclic voltammetry profiles of the half cells (Zn@Cu||Li) were collected at a scan rate of 0.5 mV s^{-1} in the scan window of −0.2 V to 1 V vs Li+/Li. Electrochemical impedance spectroscopy (EIS) and galvanostatic intermittent titration technique (GITT) were applied for kinetics characterization and diffusion coefficient determination of Li^+ for the 1Zn@Cu sample. For GITT experiment, 40 μA were applied to discharge the half cell in every 0.1 V of voltage drop followed by 110 min of relaxation. At each 0.1 V voltage interval, the impedance was measured over a frequency range of 7 MHz to 1 mHz with an applied AC signal of 10 mV amplitude. This procedure continued until the lithium plating voltage dropped below 0.1 V.

2.3. Materials characterization

Scanning electronic microscopy (SEM, EVO 50 EP, Zeiss) images were taken at an accelerating voltage of 20 kV to observe the surface morphology of the prepared anode current collectors both after full lithium plating and stripping. Cell disassembling was done in the Ar-filled glovebox and salts and electrolyte residuals were removed by washing samples with fresh dimethyl carbonate (DMC). X-ray energy dispersive spectrometer (EDS, INCA x-sight detector, Oxford instruments) was employed to extract map analysis of the surface. The phase formation after lithium deposition was investigated by using x-ray diffraction (PW1830, Kα1Cu = 1.54,058 Å, Philips). The thickness of Zn@Cu samples for all electrodes was measured by x-ray fluorescence (XRF, Fischer XAN-FD BC) for 20 s for each sample at 10 different points on the surface of each electrode and the averages are reported.

3. Results and discussion

Fig. 1a illustrates the concept of controlled Li deposition on the modified current collector. The lithiophilic zinc coating prevents irregular dendrite formation resulting in a uniform deposition of lithium on the surface. The film coating thickness versus deposition time is shown in Fig. 1b. It is observed that the electrodeposited zinc coating thickness is linearly proportional to the deposition time, as predicted by the Faraday law for electrodeposition, with a uniform coverage on the whole Zn plated area (typically 0.785 cm^2). Zinc thickness didn't exceed 1 μm to investigate the effect of a thin, light and cost-effective coating.

The first cycle of cyclic voltammetry graph (Fig. 2) of the half cells including bare Cu and Zn coated copper foil (1 μm) is shown to better perceive the stripping/deposition behavior. During the cathodic scan of both electrodes, in the inset figure, the peaks at 0.7 V are likely attributed to the electrolyte decomposition to form solid electrolyte interphase (SEI). The cathodic peaks of 1Zn@Cu electrode below 0.6 V seemed to be the rapid alloying process of Li with Zn and Li plating starts

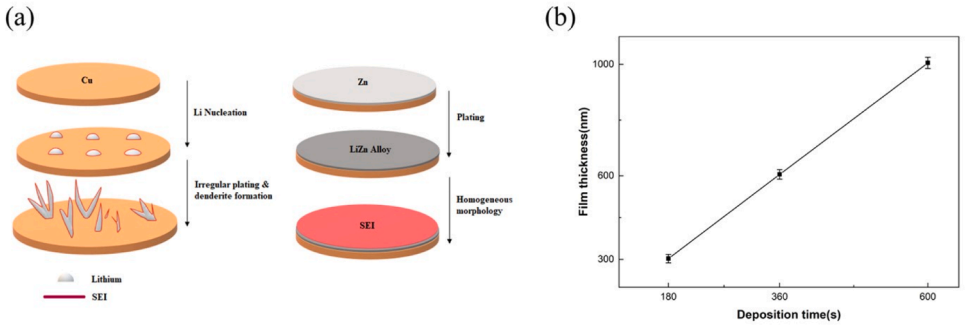

Fig. 1. a) Schematic presentation of lithium deposition on a bare Cu foil and zinc modified foil. Inhomogeneous nucleation of Li on the bare Cu leads to irregular dendritic Li growth. Zinc layer forms lithiophilic thin coating providing a uniform Li nucleation and growth. b) Plot of deposited film thickness vs. deposition time.

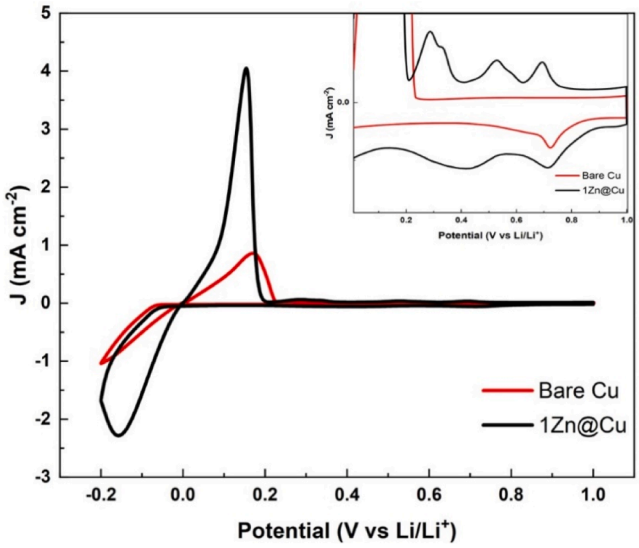

Fig. 2. Cyclic voltammetry of the bare Cu foil and the 1Zn@Cu substrate in 1.0 M LiTFSI in 1,3-dioxolane/1,2-dimethoxyethane (DOL/DME) with 3wt% LiNO3. Scan rate of 0.5 mV s^{-1}.

negative potential values. Upon the anodic scan, a broad peak around 0.2 V for both electrodes were attributed to the Li stripping process. Moreover, for the 1Zn@Cu electrode the stripping peak showed remarkably improved current peaks as result of the greater extent of Li deposition occurred in the cathodic scan. As the anodic potential was reversed to the more positive values, three anodic current peaks around 0.3, 0.5 and 0.7 V appeared only for Zn coated electrode. The presence of these three distinct peaks in the anodic curve of the coated sample are associated to the oxidation of lithium from the Li-Zn complex alloyed compound [49].

The SEM images of the pristine copper foil and the as-deposited 1Zn@Cu samples are reported in Fig. 3a,b. As seen, a smoother and flattened Zn coated layer was achieved in comparison to the pristine bare Cu substrate. Also, a more direct morphological comparison of the Zn coated samples (tilted surface) is shown in Fig. S2a-d. The 1Zn@Cu (Fig. S2c) displays a consistent, smooth and even roughness, while the 0.3Zn@Cu (Fig. S2a) is more irregular and non-uniform. SEM images of the electrodes were taken both in the fully Li-plated (Fig. 3d-g) and fully Li-stripped state (Fig. 3 h-k) after 3 cycles. The bare Cu electrode foil clearly exhibited rough porous lithium-plated morphology. Irregular geometries of lithium deposits were also observed on the 0.3Zn@Cu coated electrode after Li plating. With the increase of the zinc layer thickness (Fig. 3f,g), the surface is more homogeneously covered by dense lithium deposits, taking into account that increasing the Zn thickness, lithium was partially consumed for the Li-Zn alloying at the expense of lower quantity of plated Li, under a limited capacity of 1 mAh cm^{-2}. SEM images of the fully stripped state (Fig. 3h-k), revealed there were still some lithium spots (highlighted dashed red lines) on the surface of neat Cu and 0.3Zn@Cu, indicating that not all the lithium was stripped out. These residual lithium spots were associated to the low columbic efficiency cycles. In contrast, the 0.6Zn@Cu and 1Zn@Cu (Fig. 3j, k) showed a porous structure and no evident residual lithium spots observed on the surface, as result of the smoother Li plated layer that facilitate its complete dissolution during the oxidation steps

In order to better perceive the alloying and deposition mechanism of lithium on the zinc coated substrate, XRD analysis was performed on fully Li-plated neat Cu and 1Zn@Cu electrodes (Fig 3c). The XRD patterns relative to 1Zn@Cu sample revealed the presence of Li_1Zn_1 alloy, associated to diffraction peaks at 41.07°, 48.66° and 59.53° (JPCDS card 98–010–4793 and 98–064–2409 respectively). The absence of a Zn peak in 1Zn@Cu suggests complete alloying of the Zn layer with Li during the plating process, forming LiZn. The magnified XRD plot shows two small peaks at 37.4° and 56.8° (JPCDS card 98–019–2089) associated to $Li_{0.96}Zn_{3.04}$ phase (Fig. S3). This indicates that the plating process was successful, with all Zn effectively alloyed with Li. Additionally, the absence of other intermetallic phases and compositions such as Li_xZn_y (e.g., Li_2Zn_3, Li_2Zn_5) indicates rapid phase-transformation reactions between Li and Zn. [50]. Peaks at 43.3°and 50.4° (JPCDS card 00–004–0836) both correspond to copper foil of the current collector. In principle, crystal nucleation and growth are highly affected by crystal structure mismatch between Li metal ions and the substrate. Crystal nucleation and growth of lithium during plating are highly affected both by crystal structure mismatch between Li and the substrate and the adsorption energy of Li ions to the substrate. The minimum crystal lattice mismatch or preferred values of Li ion adsorption energy ($\Delta G_{ads} \sim 0$ eV) defines the lithiophilicity of the substrate. In this regard, LiZn alloy, formed at a potential positive than Li plating, provides both a BCC crystal structure theoretically promoting the epitaxial growth of pure Li and a ΔG_{ads} that match the required values [51,52].

To reveal the lithiophilic degree of the substrate, nucleation overpotential should be measured and obtained as the voltage difference between the minimum voltage point and the plateau potential value [53].

An abrupt decrease in voltage by −85 mV was detected on the bare copper electrode during the first cycle of Li plating at a current density of 0.25 mA cm^{-2} as shown in Fig. 4a. The potential then gradually increased and remained at a plateau so that the nucleation overpotential on the bare Cu was estimated as 44.5 mV, while for the other Zn coated electrodes it was 17.6 mV, 18 mV and 16.8 mV for 0.3Zn@Cu, 0.6Zn@Cu and 1Zn@Cu respectively. Fig. 4b shows the nucleation overpotential of all electrodes at different current densities of 0.1, 0.25, 0.5 and 1 mA cm^{-2}.

It was observed that by the increase of the Zn layer thickness on the bare copper, the nucleation overpotential decreased no matter what the current density was. It can be inferred that the Zn layer can promote the

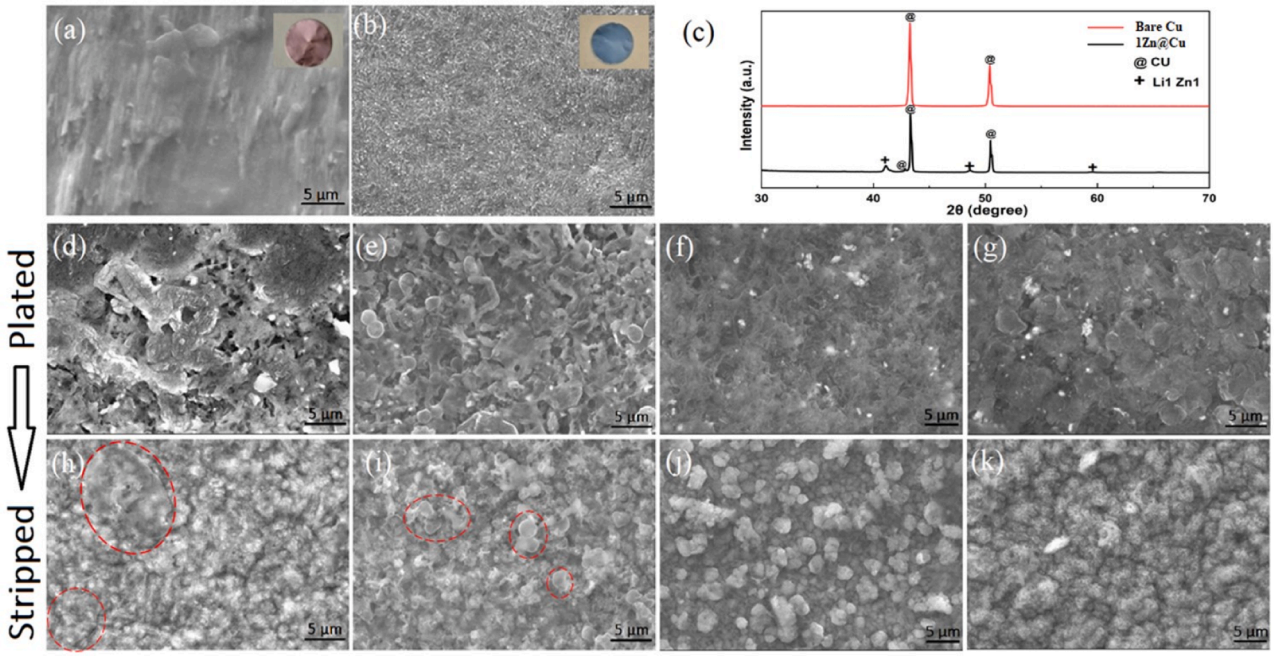

Fig. 3. SEM images of (a) pristine copper foil; (b) as-deposited 1Zn@Cu. (c) XRD patterns of fully Li-plated neat Cu and 1Zn@Cu electrodes. SEM images of fully Li-plated (d) bare Cu foil; (e) 0.3Zn@Cu; (f) 0.6Zn@Cu; (g) 1Zn@Cu. SEM images of Fully Li-stripped (h) bare Cu foil; (i) 0.3Zn@Cu; (j) 0.6Zn@Cu; (k) 1Zn@Cu. Insets in Fig (a) and (b) show pictures of the pristine Cu foil and 1Zn@Cu respectively.

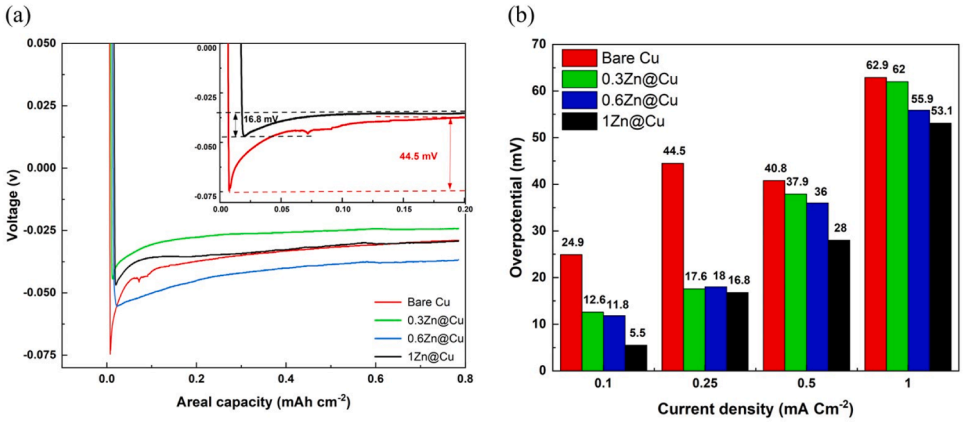

Fig. 4. (a) Plating/stripping curves of bare cu foil, 0.3Zn@Cu, 0.6Zn@Cu and 1Zn@Cu cells, inset showing the Li nucleation region of the bare Cu and 1Zn@Cu cells. (b) The Li nucleation overpotential for bare Cu foil, 0.3Zn@Cu, 0.6Zn@Cu and 1Zn@Cu cells of different current densities.

Li nucleation and can provide more electroactive surface area leading to the reduced local current density [54]. In contrast, the bare electrode was characterized by a non-uniform distribution of the current density across the surface resulting in uneven distribution of Li nucleation and growth during deposition. Consequently, even in higher current densities for Li plating, Li_1Zn_1 phase provides lithophilic Zn sites and better electrochemical behavior [55]. The ratio of Li ions (Li^+) stripped out from the anode to the Li ions plated back onto it at each platting/-stripping cycle is defined by coulombic efficiency (CE). In this regard, irreversible reactions at the anode surface like SEI thickening, electrolyte decomposition and dendrite formation may reduce the CE [56]. The CE of the bare Cu electrode decayed rapidly after 59 cycles and decreased below 90 % at even low current density of 0.5 mA cm^{-2} indicating a poor reversibility of the lithium plating process (Fig. 5a). Conversely, the Zn coated electrodes of 0.3Zn@Cu and 0.6Zn@Cu achieved 69 (at 0.5 mA cm^{-2}) and 201 cycles (in the first 180 cycles at 0.5 mA cm^{-2} and the remaining ones at 1 mA cm^{-2}) respectively, with the same areal capacity of 1 mAh cm^{-2}. However, the half-cell including the thicker Zn layer (1Zn@Cu) was more stable than the other electrodes and could maintain a significant CE above 90 % for the first 180 cycles at 0.5 mA cm^{-2} and cycled at CE > 95 % up to 275 cycles, after which a quick drop in CE occurred. Under higher stress cycling at 1 mA cm^{-2}, the 1Zn@Cu electrode endured more cycles than 0.6Zn@Cu, but both experienced a sharp decrease in %CE at this current density. The CEs of the 1Zn@Cu and 0.6Zn@Cu electrodes showed much less fluctuations and were more stable in comparison to the bare Cu and 0.3Zn@Cu cells. Hence, the Zn layer could stabilize the plating/stripping process in further cycles to avoid dendritic structure leading to columbic efficiency drop. Moreover, the mossy dendrite as shown in SEM images of the bare Cu (Fig. 3d) led to an increased surface area that accelerate electrolyte decomposition and loss of CE.

The V-t profile of the long-term plating-striping cycling test are reported in Fig 5b. The fluctuating voltage hysteresis observed during Li-plating/stripping on the bare Cu substrate was caused by the unstable

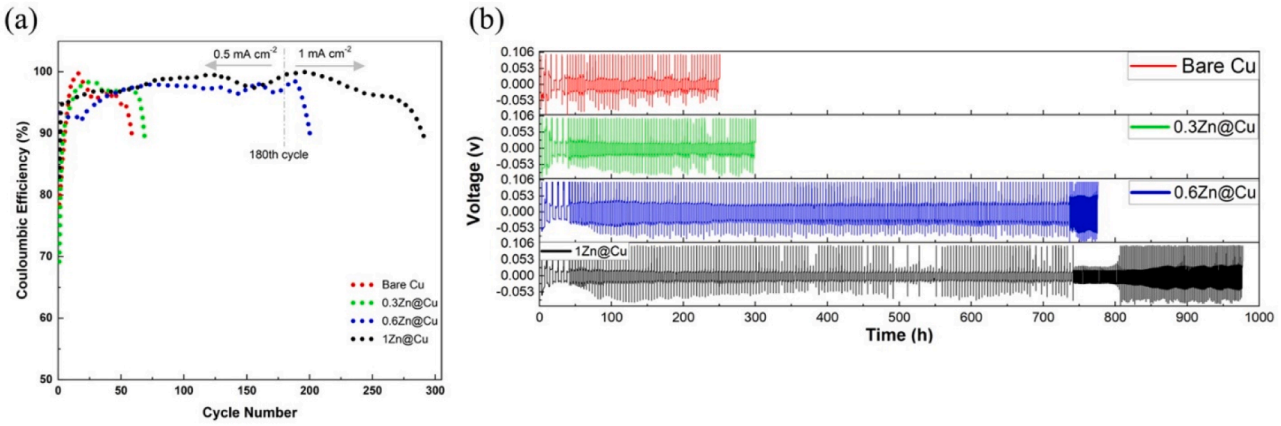

Fig. 5. (a) Coulombic efficiency (CE%) of plating/stripping tests. (b) The V-t profile of the long-term plating-striping cycling test.

interface between Li and the bare Cu. The cycling life was relatively short, lasting less than 240 h. This is because lithiophobic bare Cu forms high nucleation barriers, which lead to unstable nucleation and growth. This occurs following the formation of dead lithium and a significant increase in dendrite-induced resistance during cycling. Conversely, when using zinc coated electrodes, the voltage hysteresis was

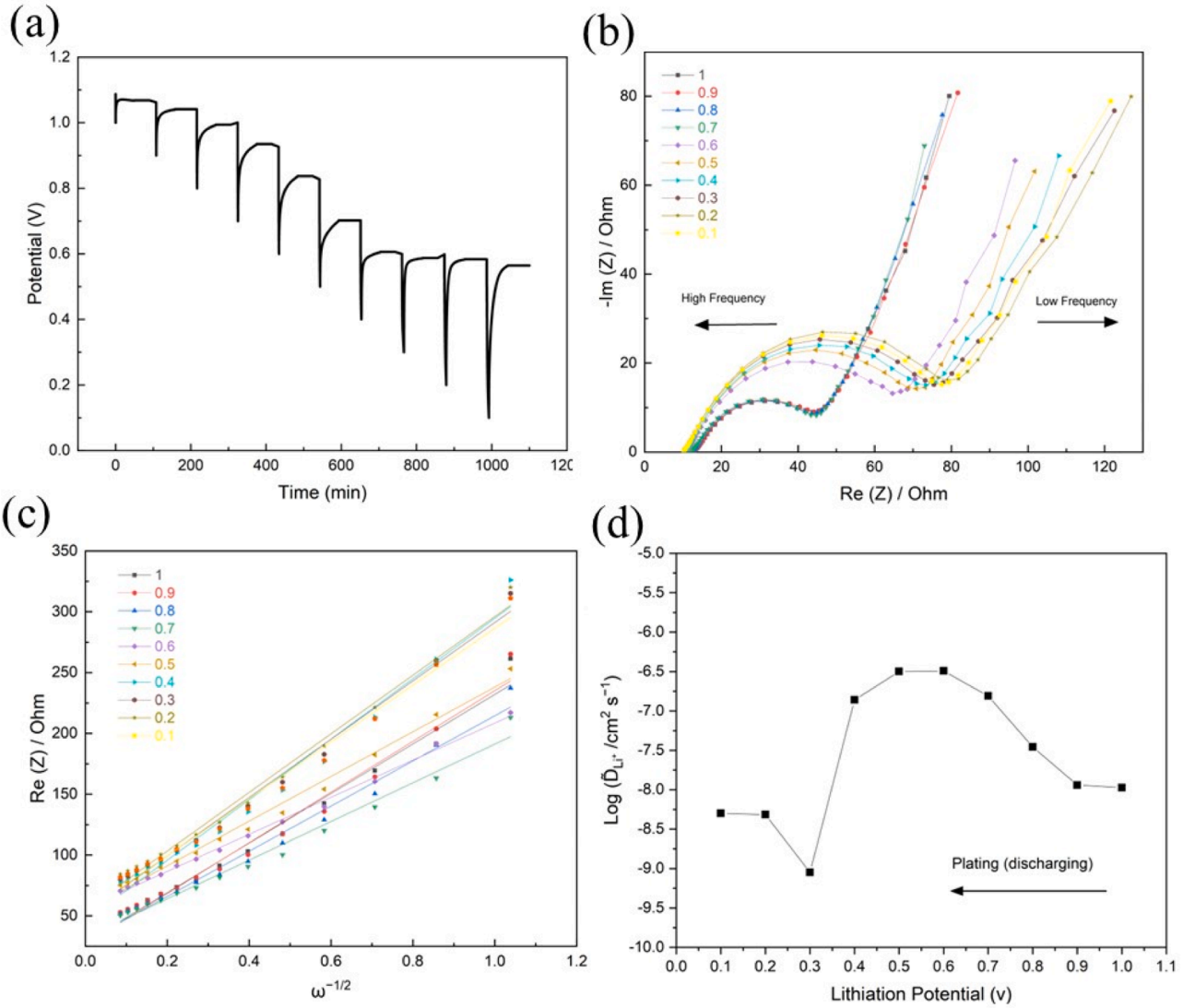

Fig. 6. GITT experiment by EIS (a) The titration steps of galvanostatic discharging by 40 μA applied current following 110 min of open circuit condition after each 0.1 V voltage drop. (b) Nyquist plot of 1Zn@Cu at different plating potentials. (C) The plots of the Z′ as a function of the inverse square root of angular frequency at different voltages in the Warburg region. (d) The calculated diffusion coefficients within plating process at different lithiation potentials by GITT.

consistently stable and there were no irregular oscillations. The 0.3Zn@Cu cell exhibited significantly improved cycling stability, maintaining a consistent voltage amplitude and minimal voltage fluctuations throughout 300 h of cycling. However, short cycling behavior of 0.3Zn@Cu electrode can be attributed to the instability of the SEI layer and to internal soft short circuit by Li dendrite propagation. Both 0.6Zn@Cu and 1Zn@Cu half cells showed superior stable plating/stripping behavior. These results suggest that an increase of Zn content can provide a more efficient interfacial contact between the anode and the electrolyte attributed to the formation of a smoother Li-metal surface, facilitated by the electrochemically formed Zn-Li alloy. When the applied current density increased from 0.5 mA cm^{-2} to 1 mA cm^{-2} minimal overpotential increase was also observed at the stage of the applied current density of 1 mA cm^{-2}, around 740 h for 0.6Zn@Cu and 1Zn@Cu cells. However, this increase was much lower and more stable for 1Zn@Cu. The 0.6Zn@Cu and 1Zn@Cu cell could maintain 775 h and 970 h of stable long-cycling profile without any short and the gradual drop in CE could be associated to internal impedance increase due to excessive SEI accumulation rather than to local short circuits, as suggested by the more and more extensive voltage hysteresis evident for the Zn@Cu V-t profile after few tens of cycles at 1 mA cm^{-2}. A fast Li^+ diffusion (D), along with electronic conductivity of the electrode, improves the electrochemical reaction kinetics. The diffusion of Li^+ in Zn during the electrochemical alloying happens by solid state diffusion that has slower kinetics with respect to the conventional Li^+ intercalation. As consequence, Li^+ diffusion in the alloy greatly controls the overall cell performance, since the catalytic surface is not Zn itself but the Li_1Zn_1 alloy [57]. Thus, the 1Zn@Cu electrode was subjected to a combination of GITT and EIS techniques to assess the diffusion coefficient of lithium ions. The titration steps of galvanostatic discharging are shown in Fig. 6a. After the current was stopped, an increase in voltage occurred due to the even distribution of Li^+ ions within the solid phase to attain a stable equilibrium voltage level. Nyquist plots for Zn layer with a step of 0.1 V of plating potential is shown in Fig. 6b. Each Nyquist plot is composed of a semicircle in the high frequency region and a linear trend with an inclination of around 45° observed within a low and medium frequency range. The high-frequency semicircle corresponds to the charge transfer process between the electrolyte and the zinc substrate. The 45° sloped line is associated with Warburg diffusion of lithium ions into the zinc layer. The diffusion coefficient (D) of lithium was calculated using the following Equation [58–60]:

$$D_{Li} = \frac{1}{2}\left[\left(\frac{V_m}{FS\sigma}\right)\left(\frac{dE}{d\delta}\right)\right]^2 \quad (1)$$

Where D_{Li} ($cm^2\ s^{-1}$) is the Li-ion chemical diffusion coefficient, V_m ($cm^3\ mol^{-1}$) is the mole volume of active material, F is Faraday constant (96,486 C mol^{-1}), S (cm^2) is the surface area of the electrode and dE/dδ is the slope of the titration curve from Fig. 6a. Also, σ ($\Omega\ Hz^2$) referred to as the Warburg factor, obtained from the slope of the linear correlation between Z′ or $-Z''$ and the square root of angular frequency ($\omega^{-1/2}$) in Fig. 6c. Fig. 6d shows the diffusion coefficients (D_{Li}) of lithium ions using EIS method obtained from Eq. 1. The diffusion coefficients calculated by this method varied from 10^{-9} to 10^{-6} $cm^2\ s^{-1}$ versus a potential range of 0.1 to 1 V and increased by almost two orders of magnitude reaching its peak value of $10^{-6.5}$ $cm^2\ s^{-1}$ at around 0.6 V demonstrating that the mobility of lithium ions was relatively high through the matrix. Up to 0.4 V, the diffusion coefficient remained relatively constant and then it experienced a decline, reaching a minimum value of 10^{-9} $cm^2\ s^{-1}$ at 0.3 V, likely due to the achievement of the complete lithiation and formation of the Li_1Zn_1 alloy as detected by XRD. In fact, it seems that at the end of the discharge process around 0.3 to 0.1 V, there might be not enough space for further lithium ions to alloy with Zn or anyhow the lithium insertion becomes notably difficult. Finally, at the end of the plating process at 0.1 V, diffusion coefficient slightly increased again to a value of 10^{-8} $cm^2\ s^{-1}$. It is noteworthy to highlight that the D_{Li} values of Zn are notably higher in comparison to values obtained from EIS or GITT measurements in composite electrodes containing Sn and Sb [61–63].

4. Conclusions

In this work, we propose electrodeposited Zn coatings at different coating thickness on Cu current collector as suitable and easy approach to improve the lithium plating-stripping process. The zinc plated anode design promoted a smooth, dendrite-free lithium deposition, attributed to favorable lithium alloying on the lithophilic Zn-coated surface. The zinc layer not only provided homogeneous and dense lithium deposition, but also reduced the nucleation overpotential with respect to the bare Cu anode from 44.5 mV to 16.8 mV for the 1Zn@Cu anode at an applied current density of 0.25 mA cm^{-2}. Moreover, the 1Zn@Cu anode could maintain the coulombic efficiency above 90 % for 180 cycles at 0.5 mA cm^{-2} and 290 cycles at 1 mA cm^{-2}, indicating stability superior to bare Cu electrodes and thin Zn coating. Long-term stability was substantially enhanced. Electrodes with 0.6Zn@Cu and 1Zn@Cu substrates exhibited high cyclability for 775 and 970 h respectively. GITT revealed high diffusion coefficients (10^{-9} to 10^{-6} $cm^2\ s^{-1}$), indicative of high lithium-ion mobility in the Zn@Cu anode. Also, increasing Zn layer thickness from few hundreds of nanometers to 1 μm enhanced the electrochemical performance due to higher lithiophilic active material alloying with lithium. The results confirm that integrating lithiophilic Zn thin films onto the Cu current collector enhances the performance of AFLBs, enabled efficient lithium deposition, reduced overpotential, prolonged cycling stability, and promoted ion mobility.

CRediT authorship contribution statement

Pooria Afzali: Writing – original draft, Supervision, Methodology, Investigation, Formal analysis, Data curation, Conceptualization. **Eugenio Gibertini:** Writing – original draft, Methodology, Investigation, Formal analysis, Data curation, Conceptualization. **Luca Magagnin:** Writing – original draft, Validation, Supervision, Resources, Project administration, Methodology, Conceptualization.

Declaration of competing interest

The authors declare that they have no known competing financial interests or personal relationships that could have appeared to influence the work reported in this paper.

Data availability

Data will be made available on request.

Supplementary Materials

Supplementary material associated with this article can be found in the online version at doi:10.1016/j.electacta.2024.144190.

References

[1] S. Maddukuri, D. Malka, M.S. Chae, Y. Elias, S. Luski, D. Aurbach, On the challenge of large energy storage by electrochemical devices, Electrochim. Acta 354 (2020) 136771, https://doi.org/10.1016/j.electacta.2020.136771.
[2] M. Gebhardt, J. Beck, M. Kopyto, A. Spieske, Determining requirements and challenges for a sustainable and circular electric vehicle battery supply chain: a mixed-methods approach, Sustain. Prod. Consum. 33 (2022) 203–217, https://doi.org/10.1016/j.spc.2022.06.024.
[3] Y. Guo, H. Li, T. Zhai, Reviving lithium-metal anodes for next-generation high-energy batteries, Adv. Mater. 29 (2017) 1–25, https://doi.org/10.1002/adma.201700007.
[4] Y. Wu, L. Xie, H. Ming, Y. Guo, J.Y. Hwang, W. Wang, X. He, L. Wang, H. N. Alshareef, Y.K. Sun, J. Ming, An empirical model for the design of batteries with

high energy density, ACS. Energy Lett. 5 (2020) 807–816, https://doi.org/10.1021/acsenergylett.0c00211.
[5] C.Y. Wang, T. Liu, X.G. Yang, S. Ge, N.V. Stanley, E.S. Rountree, Y. Leng, B. D. McCarthy, Fast charging of energy-dense lithium-ion batteries, Nature 611 (2022) 485–490, https://doi.org/10.1038/s41586-022-05281-0.
[6] V.V.K. Lanjapalli, F.J. Lin, S. Liou, S. Hosseini, C.L. Huang, Y.S. Chen, Y.Y. Li, Semi-infused lithium anode for advanced Li metal batteries, Electrochim. Acta 410 (2022) 139976, https://doi.org/10.1016/j.electacta.2022.139976.
[7] D. Zhuang, X. Huang, Z. Chen, H. Wu, L. Sheng, M. Zhao, Y. Bai, G. Liu, H. Xue, T. Wang, Y. Chen, J. He, A novel artificial film of lithiophilic polyethersulfone for inhibiting lithium dendrite, Electrochim. Acta 403 (2022) 139668, https://doi.org/10.1016/j.electacta.2021.139668.
[8] T. Melsheimer, M. Morey, A. Cannon, E. Ryan, Modeling the effects of pulse plating on dendrite growth in lithium metal batteries, Electrochim. Acta 433 (2022) 141227, https://doi.org/10.1016/j.electacta.2022.141227.
[9] S.K. Merso, T.M. Tekaligne, H.H. Weldeyohannes, Y. Nikodimos, K.N. Shitaw, S. K. Jiang, C.J. Huang, Z.T. Wondimkun, B.A. Jote, L. Wichmann, G. Brunklaus, M. Winter, S.H. Wu, W.N. Su, C.Y. Mou, B.J. Hwang, An in-situ formed bifunctional layer for suppressing Li dendrite growth and stabilizing the solid electrolyte interphase layer of anode free lithium metal batteries, J. Energy Storage 56 (2022) 105955, https://doi.org/10.1016/j.est.2022.105955.
[10] G. Liu, Y. Li, L. Zhang, H. Tao, X. Yang, In situ construction of high lithiophilic lithium phosphide protective layer for stable lithium metal anode, Electrochim. Acta 471 (2023) 143413, https://doi.org/10.1016/j.electacta.2023.143413.
[11] J. Zhang, A. Khan, X. Liu, Y. Lei, S. Du, L. Lv, H. Zhao, D. Luo, Research progress of anode-free lithium metal batteries, Crystals. (Basel) (2022) 12, https://doi.org/10.3390/cryst12091241.
[12] C. Zhao, Z. Yan, B. Zhou, Y. Pan, A. Hu, M. He, J. Liu, J. Long, Identifying the role of Lewis-base sites for the chemistry in lithium-oxygen batteries, Angewandte Chemie - Int. Ed. 62 (2023), https://doi.org/10.1002/anie.202302746.
[13] A. Hu, W. Chen, F. Li, M. He, D. Chen, Y. Li, J. Zhu, Y. Yan, J. Long, Y. Hu, T. Lei, B. Li, X. Wang, J. Xiong, Nonflammable polyfluorides-anchored quasi-solid electrolytes for ultra-safe anode-free lithium pouch cells without thermal runaway, Adv. Mater. 35 (2023), https://doi.org/10.1002/adma.202304762.
[14] T.M. Hagos, H.K. Bezabh, C.J. Huang, S.K. Jiang, W.N. Su, B.J. Hwang, A powerful protocol based on anode-free cells combined with various analytical techniques, Acc. Chem. Res. 54 (2021), https://doi.org/10.1021/acs.accounts.1c00528.
[15] C.J. Huang, Y.C. Hsu, K.N. Shitaw, Y.J. Siao, S.H. Wu, C.H. Wang, W.N. Su, B. J. Hwang, Lithium oxalate as a lifespan extender for anode-free lithium metal batteries, ACS. Appl. Mater. Interfaces. 14 (2022) 26724–26732, https://doi.org/10.1021/acsami.2c04693.
[16] N.A. Sahalie, Z.T. Wondimkun, W.N. Su, M.A. Weret, F.W. Fenta, G.B. Berhe, C. J. Huang, Y.C. Hsu, B.J. Hwang, Multifunctional Properties of Al2O3/Polyacrylonitrile Composite Coating on Cu to Suppress Dendritic Growth in Anode-Free Li-Metal Battery, ACS. Appl. Energy Mater. 3 (2020) 7666–7679, https://doi.org/10.1021/acsaem.0c01080.
[17] Y. Li, A. Hu, X. Gan, M. He, J. Zhu, W. Chen, Y. Hu, T. Lei, F. Li, Y. Li, Y. Fan, F. Wang, M. Zhou, A. Wen, B. Li, Synergy of in-situ heterogeneous interphases tailored lithium deposition, Nano Res. 16 (2023) 8304–8312, https://doi.org/10.1007/s12274-022-5004-0.
[18] A. Hu, W. Chen, Y. Pan, J. Zhu, Y. Li, H. Yang, R. Li, B. Li, Y. Hu, D. Chen, F. Li, J. Long, C. Yan, T. Lei, N, F-enriched inorganic/organic composite interphases to stabilize lithium metal anodes for long-life anode-free cells, J. Colloid. Interface Sci. 648 (2023) 448–456, https://doi.org/10.1016/j.jcis.2023.06.021.
[19] V. Nilsson, A. Kotronia, M. Lacey, K. Edström, P. Johansson, Highly concentrated LiTFSI-EC electrolytes for lithium metal batteries, ACS. Appl. Energy Mater. 3 (2020) 200–207, https://doi.org/10.1021/acsaem.9b01203.
[20] T.T. Beyene, H.K. Bezabh, M.A. Weret, T.M. Hagos, C.-J. Huang, C.-H. Wang, W.-N. Su, H. Dai, B.-J. Hwang, Concentrated dual-salt electrolyte to stabilize Li metal and increase cycle life of anode free Li-metal batteries, J. Electrochem. Soc. 166 (2019) A1501–A1509, https://doi.org/10.1149/2.0731908jes.
[21] B. Yang, Y. Pan, T. Li, A. Hu, K. Li, B. Li, L. Yang, J. Long, High-safety lithium metal pouch cells for extreme abuse conditions by implementing flame-retardant perfluorinated gel polymer electrolytes, Energy Storage Mater. 65 (2024), https://doi.org/10.1016/j.ensm.2023.103124.
[22] S. Pal, X. Zhang, B. Babu, X. Lin, J. Wang, A. Vlad, Materials, electrodes and electrolytes advances for next-generation lithium-based anode-free batteries, Oxford Open Mater. Sci. 2 (2022), https://doi.org/10.1093/oxfmat/itac005.
[23] M. Mao, X. Ji, Q. Wang, Z. Lin, M. Li, T. Liu, C. Wang, Y.-S. Hu, H. Li, X. Huang, L. Chen, L. Suo, Anion-enrichment interface enables high-voltage anode-free lithium metal batteries, Nat. Commun. 14 (2023) 1082, https://doi.org/10.1038/s41467-023-36853-x.
[24] C. Zhao, Y. Pan, R. Li, A. Hu, B. Zhou, M. He, J. Chen, Z. Yan, Y. Fan, N. Chen, M. Liu, J. Long, A safe anode-free lithium metal pouch cell enabled by integrating stable quasi-solid electrolytes with oxygen-free cathodes, Chem. Eng. J. 463 (2023), https://doi.org/10.1016/j.cej.2023.142386.
[25] A. Hu, W. Chen, X. Du, Y. Hu, T. Lei, H. Wang, L. Xue, Y. Li, H. Sun, Y. Yan, J. Long, C. Shu, J. Zhu, B. Li, X. Wang, J. Xiong, An artificial hybrid interphase for an ultrahigh-rate and practical lithium metal anode, Energy Environ. Sci. 14 (2021) 4115–4124, https://doi.org/10.1039/d1ee00508a.
[26] X. Ji, D.Y. Liu, D.G. Prendiville, Y. Zhang, X. Liu, G.D. Stucky, Spatially heterogeneous carbon-fiber papers as surface dendrite-free current collectors for lithium deposition, Nano Today 7 (2012) 10–20, https://doi.org/10.1016/j.nantod.2011.11.002.
[27] B. Zhou, T. Li, A. Hu, B. Li, R. Li, C. Zhao, N. Chen, M. He, J. Liu, J. Long, Scalable fabrication of ultra-fine lithiophilic nanoparticles encapsulated in soft buffered hosts for long-life anode-free Li2S-based cells, Nanoscale 15 (2023) 15318–15327, https://doi.org/10.1039/d3nr03035k.
[28] D. Zhang, A. Dai, M. Wu, K. Shen, T. Xiao, G. Hou, J. Lu, Y. Tang, Lithiophilic 3D Porous CuZn current collector for stable lithium metal batteries, ACS. Energy Lett. 5 (2020) 180–186, https://doi.org/10.1021/acsenergylett.9b01987.
[29] H.N. Umh, J. Park, J. Yeo, S. Jung, I. Nam, J. Yi, Lithium metal anode on a copper dendritic superstructure, Electrochem. Commun. 99 (2019) 27–31, https://doi.org/10.1016/j.elecom.2018.12.015.
[30] A. Varzi, L. Mattarozzi, S. Cattarin, P. Guerriero, S. Passerini, 3D Porous Cu–Zn alloys as alternative anode materials for Li-Ion Batteries with Superior Low T Performance, Adv. Energy Mater. 8 (2018) 1701706, https://doi.org/10.1002/aenm.201701706.
[31] X. Fan, Y. Li, C. Luo, S. Luo, B. Huang, S. Liu, W. Sun, Vertically aligned MnO2 nanosheets on carbon fiber cloth as lithiophilic host enables dendrite-free lithium metal anode, Electrochim. Acta 464 (2023) 142896, https://doi.org/10.1016/j.electacta.2023.142896.
[32] N. Shin, M. Kim, J. Ha, Y.-T. Kim, J. Choi, Flexible anodic SnO2 nanoporous structures uniformly coated with polyaniline as a binder-free anode for lithium ion batteries, J. Electroanal. Chem. 914 (2022) 116296, https://doi.org/10.1016/j.jelechem.2022.116296.
[33] S. Koul, Y. Morita, F. Fujisaki, H. Ogasa, Y. Fujiwara, A. Kushima, Effect of liquid metal coating on improved cycle performance of anode-free lithium metal battery, J. Electrochem. Soc. 169 (2022) 020542, https://doi.org/10.1149/1945-7111/ac4ea5.
[34] S. Jin, Y. Jiang, H. Ji, Y. Yu, Advanced 3D current collectors for lithium-based batteries, Adv. Mater. 30 (2018) 1802014, https://doi.org/10.1002/adma.201802014.
[35] K. Yan, Z. Lu, H.W. Lee, F. Xiong, P.C. Hsu, Y. Li, J. Zhao, S. Chu, Y. Cui, Selective deposition and stable encapsulation of lithium through heterogeneous seeded growth, Nat. Energy (2016) 1, https://doi.org/10.1038/NENERGY.2016.10.
[36] C. Zhang, W. Lv, G. Zhou, Z. Huang, Y. Zhang, R. Lyu, H. Wu, Q. Yun, F. Kang, Q. H. Yang, Vertically Aligned Lithiophilic CuO Nanosheets on a Cu collector to stabilize lithium deposition for lithium metal batteries, Adv. Energy Mater. 8 (2018), https://doi.org/10.1002/aenm.201703404.
[37] Y. Zhang, B. Liu, E. Hitz, W. Luo, Y. Yao, Y. Li, J. Dai, C. Chen, Y. Wang, C. Yang, H. Li, L. Hu, A carbon-based 3D current collector with surface protection for Li metal anode, Nano Res. 10 (2017) 1356–1365, https://doi.org/10.1007/s12274-017-1461-2.
[38] Y. Jiang, Z. Wang, C. Xu, W. Li, Y. Li, S. Huang, Z. Chen, B. Zhao, X. Sun, D. P. Wilkinson, J. Zhang, Atomic layer deposition for improved lithiophilicity and solid electrolyte interface stability during lithium plating, Energy Storage Mater. 28 (2020) 17–26, https://doi.org/10.1016/j.ensm.2020.01.019.
[39] H. Zheng, Q. Zhang, Q. Chen, W. Xu, Q. Xie, Y. Cai, Y. Ma, Z. Qiao, Q. Luo, J. Lin, L. Wang, B. Qu, B. Sa, D.L. Peng, 3D lithiophilic-lithiophobic-lithiophilic dual-gradient porous skeleton for highly stable lithium metal anode, J. Mater. Chem. a Mater. 8 (2020) 313–322, https://doi.org/10.1039/c9ta09505e.
[40] Q. Xu, J. Lin, C. Ye, X. Jin, D. Ye, Y. Lu, G. Zhou, Y. Qiu, W. Li, Air-stable and dendrite-free lithium metal anodes enabled by a hybrid interphase of C60 and Mg, Adv. Energy Mater. 10 (2020) 1903292, https://doi.org/10.1002/aenm.201903292.
[41] M.S. Kim, S.H. Lee, M.-S. Kim, J.-H. Ryu, K.-R. Lee, L.A. Archer, W. Il Cho, Enabling reversible redox reactions in electrochemical cells using protected LiAl intermetallics as lithium metal anodes, Sci. Adv. 5 (2024) eaax5587, https://doi.org/10.1126/sciadv.aax5587.
[42] S. Liu, X. Zhang, R. Li, L. Gao, J. Luo, Dendrite-free Li metal anode by lowering deposition interface energy with Cu99Zn alloy coating, Energy Storage Mater. 14 (2018) 143–148, https://doi.org/10.1016/j.ensm.2018.03.004.
[43] T. Fujieda, S. Takahashi, S. Higuchi, Cycling behaviour of electrodeposited zinc alloy electrode for secondary lithium batteries, J. Power. Sources. 40 (1992) 283–289, https://doi.org/10.1016/0378-7753(92)80016-5.
[44] N. Zhang, S.H. Yu, H.D. Abruña, Regulating lithium nucleation and growth by zinc modified current collectors, Nano Res. 13 (2020) 45–51, https://doi.org/10.1007/s12274-019-2567-7.
[45] Z. Qiang, B. Liu, B. Yang, P. Ma, X. Yan, B. Wang, Preparation of three-dimensional copper-zinc alloy current collector by powder metallurgy for lithium metal battery anode, ChemElectroChem. 8 (2021) 2479–2487, https://doi.org/10.1002/celc.202100561.
[46] S. Sen Chi, Q. Wang, B. Han, C. Luo, Y. Jiang, J. Wang, C. Wang, Y. Yu, Y. Deng, Lithiophilic Zn Sites in Porous CuZn Alloy Induced Uniform Li Nucleation and Dendrite-free Li Metal Deposition, Nano Lett. 20 (2020) 2724–2732, https://doi.org/10.1021/acs.nanolett.0c00352.
[47] T.A. Nigatu, H.K. Bezabh, S.-K. Jiang, B.W. Taklu, Y. Nikodimos, S.-C. Yang, S.-H. Wu, W.-N. Su, C.-C. Yang, B.J. Hwang, An anode-free aqueous hybrid batteries enabled by in-situ Cu/Sn/Zn alloy formation on pure Cu substrate, Electrochim. Acta 443 (2023) 141883, https://doi.org/10.1016/j.electacta.2023.141883.
[48] L. Bertoli, S. Bloch, E. Andersson, L. Magagnin, D. Brandell, J. Mindemark, Combination of solid polymer electrolytes and lithiophilic zinc for improved plating/stripping efficiency in anode-free lithium metal solid-state batteries, Electrochim. Acta 464 (2023) 142874, https://doi.org/10.1016/j.electacta.2023.142874.
[49] C. Chen, Y. Yang, H. Shao, Enhancement of the lithium cycling capability using Li-Zn alloy substrate for lithium metal batteries, Electrochim. Acta 137 (2014) 476–483, https://doi.org/10.1016/j.electacta.2014.06.006.
[50] Y. Hwa, J.H. Sung, B. Wang, C.M. Park, H.J. Sohn, Nanostructured Zn-based composite anodes for rechargeable Li-ion batteries, J. Mater. Chem. 22 (2012) 12767–12773, https://doi.org/10.1039/c2jm31776a.

[51] V. Pande, V. Viswanathan, Computational screening of current collectors for enabling anode-free lithium metal batteries, ACS. Energy Lett. 4 (2019) 2952–2959, https://doi.org/10.1021/acsenergylett.9b02306.
[52] S. Li, Z. Chai, Z. Wang, C.-W. Tai, J. Zhu, K. Edström, Y. Ma, A. Multiscale, Dynamic elucidation of Li solubility in the alloy and metallic plating process, Adv. Mater. 35 (2023) 2306826, https://doi.org/10.1002/adma.202306826.
[53] A. Pei, G. Zheng, F. Shi, Y. Li, Y. Cui, Nanoscale nucleation and growth of electrodeposited lithium metal, Nano Lett. 17 (2017) 1132–1139, https://doi.org/10.1021/acs.nanolett.6b04755.
[54] K. Xu, M. Zhu, X. Wu, J. Liang, Y. Liu, T. Zhang, Y. Zhu, Y. Qian, Dendrite-tamed deposition kinetics using single-atom Zn sites for Li metal anode, Energy Storage Mater. 23 (2019) 587–593, https://doi.org/10.1016/j.ensm.2019.03.025.
[55] H. Liu, Y. Zhang, C. Wang, J.N. Glazer, Z. Shan, N. Liu, Understanding and controlling the nucleation and growth of Zn electrodeposits for aqueous zinc-ion batteries, ACS. Appl. Mater. Interfaces. 13 (2021) 32930–32936, https://doi.org/10.1021/acsami.1c06131.
[56] B. Wu, C. Chen, D.L. Danilov, Z. Chen, M. Jiang, R.-A. Eichel, P.H.L. Notten, Dual Additives for Stabilizing Li Deposition and SEI Formation in Anode-Free Li-Metal Batteries, Energy Environ. Mater. (2023) e12642, https://doi.org/10.1002/eem2.12642.
[57] Y. Zhu, S. Wu, L. Zhang, B. Zhang, B. Liao, Lithiophilic Zn 3N 2 -Modified Cu Current Collectors by a Novel FCVA Technology for Stable Anode-Free Lithium Metal Batteries, ACS. Appl. Mater. Interfaces. 15 (2023) 43145–43158, https://doi.org/10.1021/acsami.3c08109.
[58] W. Weppner, R.A. Huggins, Determination of the Kinetic Parameters of Mixed-Conducting Electrodes and Application to the System Li3Sb, J. Electrochem. Soc. 124 (1977) 1569–1578, https://doi.org/10.1149/1.2133112.
[59] J. Xie, N. Imanishi, A. Hirano, Y. Takeda, O. Yamamoto, X.B. Zhao, G.S. Cao, Determination of Li-ion diffusion coefficient in amorphous Zn and ZnO thin films prepared by radio frequency magnetron sputtering, Thin Solid Films 519 (2011) 3373–3377, https://doi.org/10.1016/j.tsf.2010.12.092.
[60] K.M. Shaju, G.V. Subba Rao, B.V.R. Chowdari, EIS and GITT studies on oxide cathodes, O2-Li(2/3)+x(Co0.15Mn0.85)O2 (x = 0 and 1/3), Electrochim. Acta 48 (2003) 2691–2703, https://doi.org/10.1016/S0013-4686(03)00317-7.
[61] M. Cochez, J. Jumas, P. Lavela, J. Morales, J. Olivier-Fourcade, J.L. Tirado, New tin-containing spinel sulfide electrodes for ambient temperature rocking chair cells 62 (1996) 101–105. https://doi.org/10.1016/S0378-7753(96)02409-3.
[62] J.O. Besenhard, M. Wachtler, M. Winter, R. Andreaus, I. Rom, W. Sitte, Kinetics of Li insertion into polycrystalline and nanocrystalline “SnSb” alloys investigated by transient and steady state techniques 81-81 (1999) 268–272. https://doi.org/10.1016/S0378-7753(99)00199-8.
[63] J. Xie, X.B. Zhao, G.S. Cao, M.J. Zhao, S.F. Su, Solvothermal synthesis and electrochemical performances of nanosized CoSb3 as anode materials for Li-ion batteries, J. Power. Sources. 140 (2005) 350–354, https://doi.org/10.1016/j.jpowsour.2004.08.027.